Natural Convection in Square Cavities with Three Active Source Configurations

G. Nardini, M. Paroncini, and R. Vitali

***Abstract*—** Laminar natural convection in a two-dimensional square cavity of side length H due to some sources on the vertical sidewalls was experimentally and numerically investigated. Main efforts were focused on the size of the sources on the fluid flow and heat transfer characteristics.

The test cell is a square cavity filled with air. Three cases are investigated: in the first case there are two identical active sources (hot and cold) on the side walls extended for the entire length H of the cell, in the second one there are two active sources of size H/2 and in the third one there are four sources of size H/4.

The experimental study was carried out through holographic interferometry in order to obtain the average Nusselt numbers at different Rayleigh numbers and the numerical study was carried out through the finite volume code Fluent 12.1.4.

The temperature distributions in the air and the heat transfer coefficients measured experimentally are compared with the numerical results. The isothermal lines, stream functions, velocity maps and average Nusselt numbers show the effect of the different heating size of the side walls to explore the fundamental fluid flow and heat transfer characteristics for natural convection in two-dimensional square enclosures.

***Keywords*—** Holographic interferometry, natural convection, numerical simulation, Nusselt number, square cavity

I. Introduction

IN recent years, the study of natural convection in enclosures has become very important because it provides a useful basis in many engineering fields such as solar collectors, building heating, insulation with double-pane windows, and cooling of electronic equipment.

Many studies of natural convection in cavities are presented in technical literature and some of these studies find that both size and position of the discrete heat source has a significant impact on natural convection heat transfer.

Poulikakos [1] and Ishihara et al. [2] studied rectangular enclosures with partially heated and cooled zones on a single sidewall.

Aydin et al. [3] numerically studied the convection of air in a rectangular enclosure with localized heating from below and the symmetrical cooling from the sides.

Ho and Chang [4] investigated natural convection heat transfer in a vertical rectangular enclosure with two-dimensional discrete heating. Ganzarolli et al. [5] investigated the case of a cavity symmetrically cooled from the sides; Ntibarufata et al. [6] numerically investigated natural convection in partitioned enclosures with localized heating from below; November et al. [7] studied rectangular enclosures heated from below and cooled along one side; Hasnaoui [8] investigated the natural convection in a rectangular cavity partially heated from below.

Paroncini et al. [9, 10] studied the influence of the position of a small heating source located at the bottom of a square cavity.

Nor Azwadi et al. [11, 12] natural convection heat transfer inside an inclined square cavity.

Tŭrkoglu and Yŭcel [13] investigated the effects of the heater and cooler location on natural convection in square cavities.

Nithyadevi et al [14] worked on natural convection heat transfer in the cavities with partially active sides for different aspect ratios.

Chu, Churchil et al [15] studied the effect of heater size, location, aspect ratio and boundary conditions on two dimensional laminar natural convection in rectangular channels.

Valencia and Frederick [16] studied heat transfer in square cavities with partially active vertical walls. Zhao, Liu et al [17] studied laminar natural convection induced by two discrete heating elements flush mounted to one vertical wall of a square cavity.

Qi-Hong Deng [18] and Nardini et al. [19] studied natural convection in square cavities due to discrete source-sink pairs.

In this paper the results of an experimental and numerical analysis are presented to explore the heat transfer characteristics for natural convection in a square enclosure with three different active source configurations.

The effect of the size of hot and cold sources located on sidewalls on natural convective heat transfer is investigated. Three different source configurations are analyzed: in the first case (l = H configuration) there are two identical active sources (hot and cold) on the side walls extended for the entire length H of the cell, in the second one (l = H/2 configuration) the hot and the cold strips of size H/2 are always kept in the middle of the side walls, while in the third one (l = H/4

G.Nardini is with the DIISM, Dipartimento di Ingegneria Industriale e Scienze Matematiche, Università Politecnica delle Marche, Via Brecce Bianche - 60131 Ancona, ITALY (corresponding author phone +390712204876, fax +390712204770, e-mail: g.nardini@univpm.it).

M.Paroncini., is with the DIISM, Dipartimento di Ingegneria Industriale e Scienze Matematiche, Università Politecnica delle Marche, Via Brecce Bianche - 60131 Ancona, ITALY (e-mail: m.paroncini@univpm.it).

R.Vitali is with the DIISM, Dipartimento di Ingegneria Industriale e Scienze Matematiche, Università Politecnica delle Marche, Via Brecce Bianche - 60131 Ancona, ITALY (e-mail: r.vitali@univpm.it).

configuration) a source pair (hot) of size H/4 is located on the left lateral wall, and the other pair (cold) is located on the right wall. For all cases the cold strips are always kept at the same temperature, the temperature of the hot sources is changed from one test to another to obtain different Rayleigh numbers. The thermal behavior of the heat transfer is experimentally measured by double-exposure holographic interferometry, while it is numerically investigated through Fluent 12.1.4 [20]. For each case studied the experimental and numerical correlation connecting the Rayleigh numbers with the corresponding Nusselt numbers are elaborated and analyzed.

NOMENCLATURE

a = Thermal diffusivity [$m^2 \cdot s^{-1}$]
g = Modulus of the gravity vector [$m \cdot s^{-2}$]
H = Square cavity side [m]
k = Thermal conductivity [$W \cdot m^{-1} \cdot K^{-1}$]
l = Heat source length [m]
L = Cavity depth in the experimental tests [m]
$\overline{Nu}$ = Average Nusselt number of the heat source
Nu_h = Local Nusselt number
Nu_{higher} = average Nusselt number of the higher source in l = H/4 configuration
Nu_{lower} = average Nusselt number of the lower source in l = H/4 configuration
Pr = Prandlt number
Ra = Rayleigh number
T = Temperature [K]
ΔT = Temperature difference between heat sources and cold strips [K]
x = Cartesian axis direction [m]
X = Dimensionless Cartesian axis direction
y = Cartesian axis direction [m]
Y = Dimensionless Cartesian axis direction

Greek symbols

β = Thermal expansion coefficient [K^{-1}]
ε = Dimensionless length of the heat source
θ = Dimensionless temperature
ρ = Density [$kg \cdot m^{-3}$]
υ = Kinematic viscosity [$m^2 \cdot s^{-1}$]

Subscripts

c = Cold wall
cal= Calculated data
exp = Experimental data
h = Hot wall
num = Numerical data

II. Experimental Set up

The experimental set up is composed by a test cell, a pneumatic auto leveling table, optical instruments, two thermostatic baths and a data acquisition system.

The test cell is a square enclosure filled with air at atmospheric pressure (Pr=0.71), the room temperature of 297 K, and a relative humidity of 50% is set.

The sides of the square cavity section have dimension H=0.05 m. The dimension of the test cell along the longitudinal direction is 0.42 m. This length is considered big enough to neglect the end effects and to work with a two-dimensional model. The set up is shown in Fig. 1.

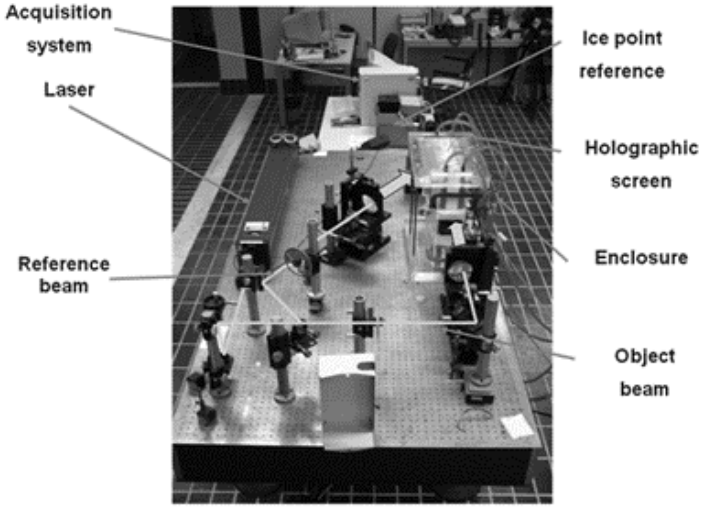

Fig.1 Holographic interferometry

In the first configuration (l = H configuration), there are two sources made of aluminum material: one strip is located on the right lateral wall and it is heated and maintained at a temperature T_h by a fluid that circulates through a thermostatic bath, while the other one is located on the left wall and it is maintained at a fixed temperature T_c. The active sources have a length of l = H and they extend on the side walls for the entire length H of the cell. In the second configuration (l = H/2 configuration), there are two sources made of the same materials of first configuration. These sources have a length of l = H/2, and they are located in the middle of the lateral walls, at a position d=0.0125 m from the floor of the enclosure. In the third configuration (l = H/4 configuration), there are four sources made of the same materials of other configurations.

The sizes of the sources are all kept the same as l = H/4: a source pair is located on the left lateral wall, and it is heated and maintained at a temperature T_h by a fluid that circulates through a thermostatic bath, while the other pair is located on the right wall that are kept at a constant temperature T_c.

For all configurations, the top and the bottom surfaces of the enclosure are made of plexiglass to prevent heat leakage through these walls. However, since this is not feasible in the experimental analysis to reproduce the adiabatic condition, the boundary condition in the numerical analysis at these surfaces was implemented in order to take into account the conductive heat flux through the plexiglass walls. The end vertical walls are made of glass to guarantee access of the laser beam.

A scheme of the enclosure for both configurations is shown in Fig. 2.

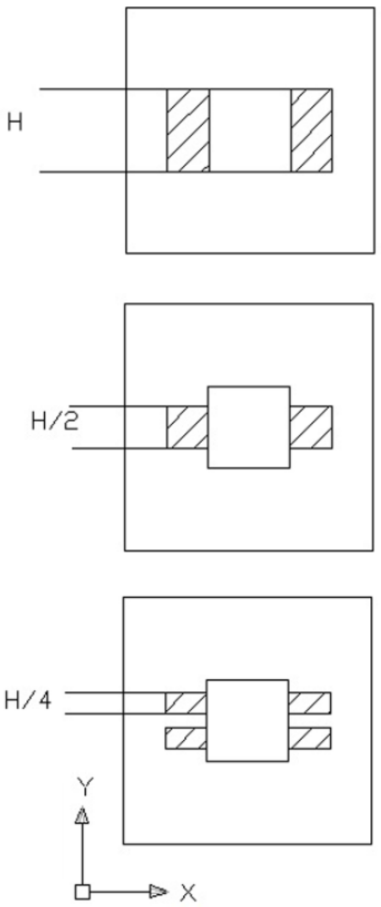

Fig.2 Test cell for l = H, l = H/2 and l = H/4 configurations

For both configurations, the temperature T_h is changed from one test to another to obtain different Rayleigh numbers, while the temperature T_c is kept constant by a fluid, which is cooled by another thermostatic bath. In this case, the temperature is kept constant during each test and was set at 291.16 K.

The thermostatic circuit is made up of two thermostats with their respective connecting pipes. The PROLINE RP1840 thermostats are manufactured by Lauda Company. Each pipe, which connects the thermostats with the inlet and outlet valves of the two sidewalls and the heater, is covered with a neoprene skin (about 0.02 m thick) to insulate it from heat loss. The thermostatic fluid is a mixture of 75% water and 25% glycol. The acquisition system is made up of several copper–constantan thermocouples for the two different configurations under test. The copper–constantan thermocouples are inserted to measure the temperature on the vertical walls and on the heated strip.

For both configurations, each thermocouple is connected with an ice point reference made by Kaye, model K170. All the thermocouples are located 1 mm under the surface of the test volume and they check the surface temperatures but do not interact with the natural convection in fact their diameters are 1 mm. The differences between the three temperatures measured on the heat sources is about 0.4 K. Unfortunately, these temperatures cannot be used directly to obtain the temperature distribution of the fringes during the interpretation of the interferograms since, because of diffraction effects, the position of both the heater and the sidewalls is uncertain. For this reason, the last thermocouple is positioned in the middle of the air region in order to give us a reference temperature for analyzing the interferograms. The results of the temperature measurements are stored by a data acquisition system.

The holographic interferometry is characterized by an optical system used to split the laser beam and to send it inside the two-dimensional cavity and on the holographic photo plates. The laser used is ‘‘Model 532-400 DPSS’’ laser, a diode-pumped, frequency-doubled Nd:YAG laser that emits an output beam at a 532 nm (green) wavelength. Both object and reference beams have a maximum diameter of 0.15 m. The optical set-up allows us to use either double-exposure or real-time holographic interferometry techniques for the steady state and temporal evolution measurements of heat transfer processes. The real-time technique is used in order to reveal the presence of plume oscillations to study the temporal evolution of transfer processes, while the double-exposure technique is used for steady-state measurements. Holographic interferometry shows the typical advantages over the classical optical techniques, such as high precision and sensitivity, very low noise level, and the possibility of displaying the temperature distribution across the whole investigated region. The interferograms are analyzed with a traveling microscope to obtain the intensity distribution. Density and temperature distribution are obtained by the usual methods of inversion. According to Hauf and Grigull [21], the expected accuracy for small fringe numbers (less than 30) can be of about 10%.

III. Numerical Set up

Fluent solution methods are known in the scientific background. In this study, the numerical simulation is developed by a finite volume code Fluent 12.1.4 using the boussinesq approximation for air and is performed with a 2d approximation

A. Segregated solver

The numerical results are carried out using the segregated solvers [16] for $10^4 < Ra < 10^5$, and then compared to the experimental data. In this study, a second order upwind implicit scheme is employed in the conservation equations as it happens for the spatial discretization. The pressure interpolation is provided by the Body Force Weighted scheme; the pressure velocity coupling is provided by the SIMPLE algorithm, and a two-dimensional model is used with the condition of laminar flow. The diffusion terms are central-differenced with a second order accuracy.

B. Numerical setting

The test cell is reproduced with real dimensions. The temperatures of the heated strips are assigned in order to obtain the same Rayleigh numbers as in the experimental analysis. The top and bottom surfaces are modeled to have conductive heat flux through the plexiglass walls.

C. Simulation procedure

The calculation starts with the steady. The numerical average Nusselt numbers ($\overline{Nu}$) on the heating elements are given by

$$\overline{Nu} = \frac{q_{tot}/A_h}{k \cdot \Delta T/H} \quad (1)$$

where q_{tot} is the heat transfer rate directly computed by Fluent, A_h is the heater surface that is considered, and k is the thermal conductivity of the air evaluated at the heating strips temperature.

The local Nusselt numbers (Nu_h) are also referred to the heat source, and they are calculated as

$$Nu_h = \frac{q''}{k \cdot \Delta T/H} \quad (2)$$

where q" is the heat flux computed by Fluent on each cell of the mesh.

IV. Results

The effect of heat sources size is investigated experimentally using the holographic interferometry both with the real time technique and the double exposure technique.

The real-time interferograms are obtained with a finite-fringe field, while an infinite-fringe field is used in the double exposure interferograms; so doing the fringe pattern shows directly the distribution of the isothermal lines.

The experimental and numerical Rayleigh numbers investigated change from about $4 \cdot 10^4$ to $4 \cdot 10^5$. The Rayleigh numbers are defined as:

$$Ra = \frac{(g \cdot \beta \cdot (T_h - T_c) \cdot H^3)}{\nu \cdot a} \quad (3)$$

The dimensionless parameters used are:

$$X = \frac{x}{H};\ Y = \frac{y}{H};\ \theta = \frac{(T - T_c)}{(T_h - T_c)};\ \varepsilon = \frac{1}{H} \quad (4)$$

The local Nusselt number – Nu(Y) – on the hot sources is calculated thanks to the expression:

$$Nu_h(Y) = -\frac{\partial \theta}{\partial X}\Big|_{X=0} \quad (5)$$

The average Nusselt number – Nu_{ave} – on the heat sources is given by the relationship:

$$\overline{Nu} = \frac{1}{\varepsilon} \int_0^{\varepsilon} Nu_h(Y)\, dY \quad (6)$$

The heat transfer rate for each source across the whole cavity is described by the average Nusselt number. The first step for the experimental study was done by the real time technique to analyze the motion development. It is important to point out that both in the real time and in the double exposure; enough time was given to the system to reach a steady configuration. The invariance of the fringes to Ra about 10^4 indicated the conduction as the major heat exchange mechanism inside this range of Ra.

In Fig. 3, it is possible to see an example of double exposure interferogram at Rayleigh number for all configurations. The fringes (Fig.3) are comparable qualitatively to the isothermal lines (Fig. 4, Fig. 5 and Fig. 6): each line is characterized by a different temperature level. It is possible to note a comparison with the distribution of the isothermal lines obtained for all configurations.

In Fig.s 3, 4, 5 and 4 c and 7, 8, and 9 it is possible to observe the isothermal lines, streamlines and velocity maps from Ra = 10^4 to Ra = 10^5. Analyzing these Fig.s (3, 4 and 5) it is observed that there is a good agreement between the experimental isothermal lines and the numerical pattern for all configurations under test. In Fig. 3 observing the isothermal lines it is possible to notice that the Nusselt number increases from H/2 to H configuration and then from H to H/4 configuration. So in H/4 configuration the heat transfer is higher than in other configurations for the same Rayleigh numbers. In the interferogram of H/4 it is possible to notice that Nusselt number is higher in the lower source than the one in the higher source.

The fringes in the high and low portion of the cavity are not perpendicular to the surface, showing that the top and bottom of the enclosure are not perfectly adiabatic.

Analyzing the interferogram for Ra = $1.79 \cdot 10^5$ (l = H), for Ra = $1.77 \cdot 10^5$ (l = H/2) and for Ra = $1.79 \cdot 10^5$ (l = H/4) it is possible to see a well-developed convective motion.

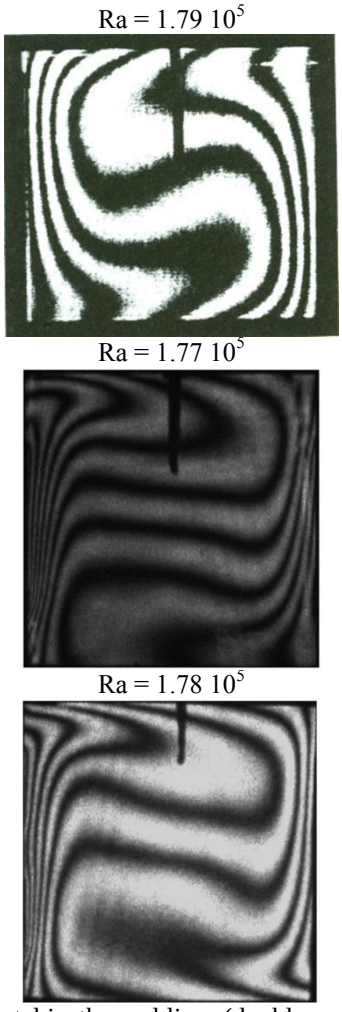

Fig.3 Experimental isothermal lines (double exposure interferograms) for ΔT = 15 K for l= H on the top and l= H/2 in the center and l = H/4 on the bottom

In fact owing to the increase in buoyancy, motion intensity increases, which implies that the heated fluid comes close to the cooled wall thus bringing to larger temperature gradients at

the wall as also testified by the increased warping of the isotherms near the cold strips. For all configurations there are few fringes on the internal zone of the cavity where the temperature gradient is lower than the one near the heat strips. This behavior shows a reduction of the heat transfer between the lateral region and the central one of the cavity and it is also confirmed by the numerical isothermal lines (Fig.s 4, 5 and 6). In fact it is observed that there are more fringes near hot sources and the temperature gradient increases.

In the numerical stream functions, Fig.s 7, 8 and 9, for Ra = $6.51 \cdot 10^4$ (l = H), for Ra = $6.19 \cdot 10^4$ (l = H/2) and for Ra = $5.73 \cdot 10^4$ (l = H/4) it is possible to see a monocellular motion. The strength of the buoyancy effect is not enough strong to create some separate recirculation zones and consequently the Nusselt numbers are low. Then for Ra > 10^5 it is possible to note the existence of some recirculation zones: their size changes with the increase of the Rayleigh number for all configurations: for Ra =$2.31 \cdot 10^5$ (l = H and l = H/4) there is only recirculation zone for Ra = $2.28 \cdot 10^5$ (l = H/2) there are two symmetrical recirculation zones.

Observing the streamlines (Fig.s7, 8 and 9) and the velocity maps (Fig.s 10, 11 and 12) it is possible to notice that the velocity fields grow with the Rayleigh numbers.

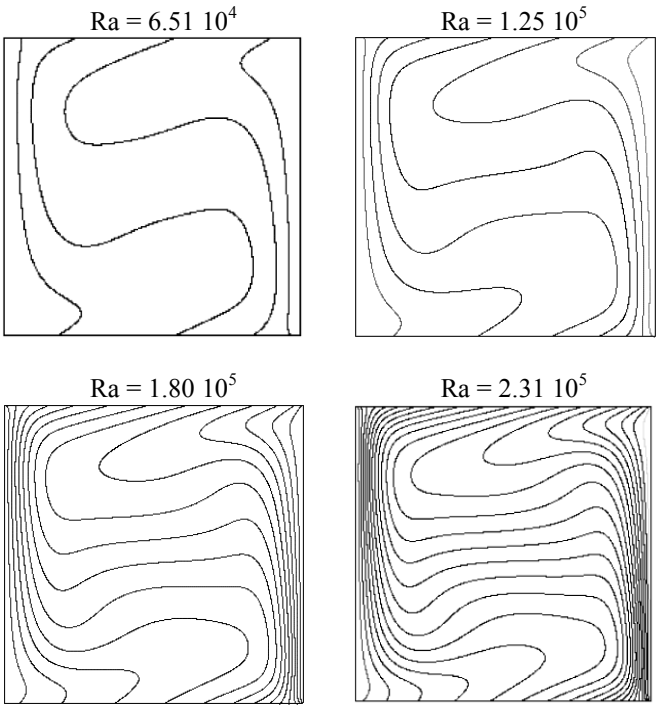

Fig.4 Numerical isothermal lines for l = H

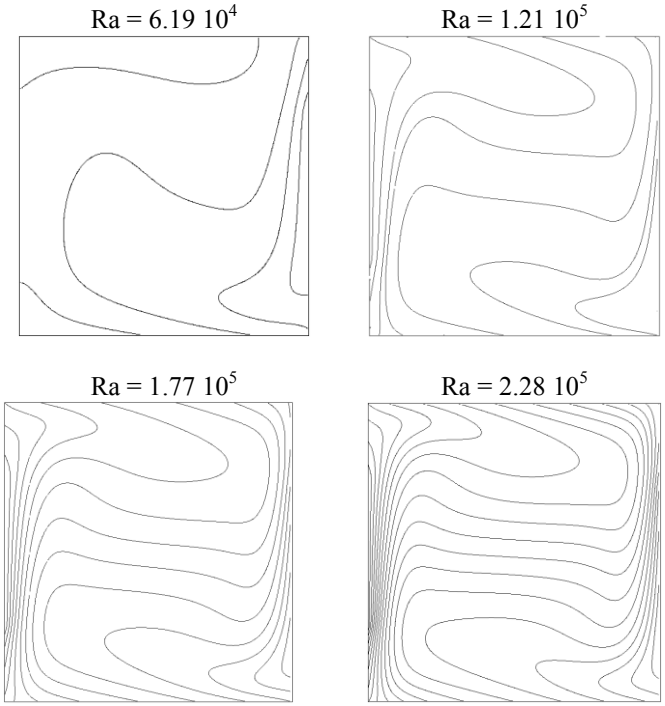

Fig.5 Numerical isothermal lines for l = H/2

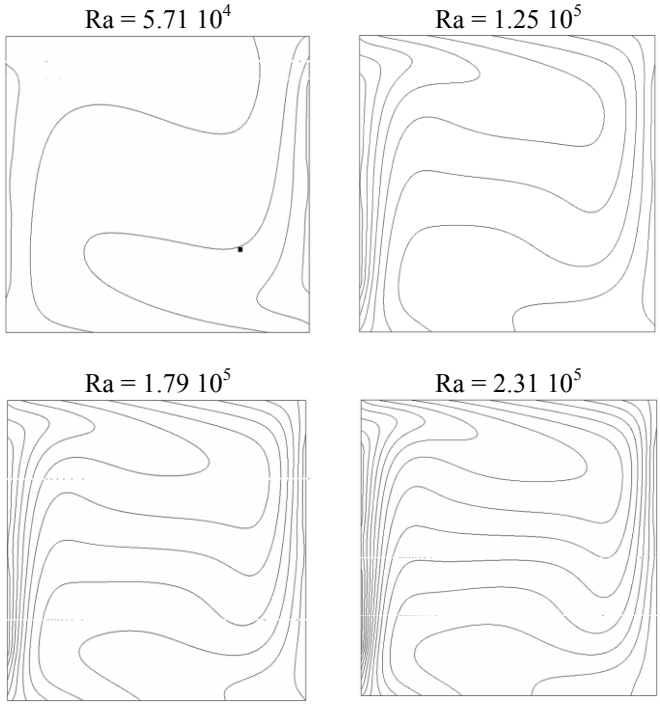

Fig.6 Numerical isothermal lines for l = H/4

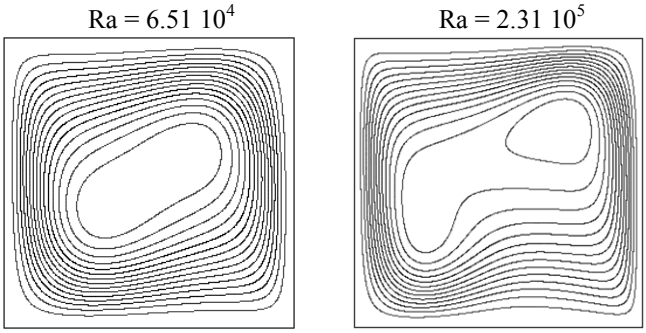

Fig.7 Numerical streamlines for l = H

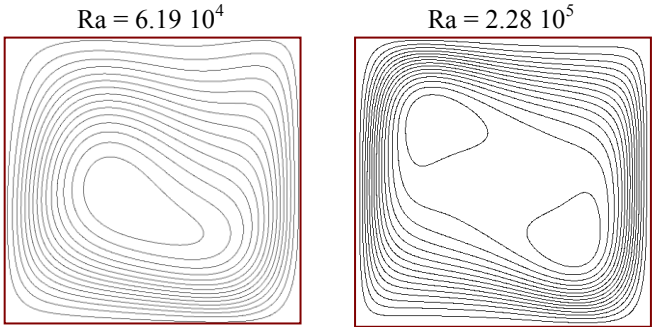

Fig.8 Numerical streamlines for l = H/2

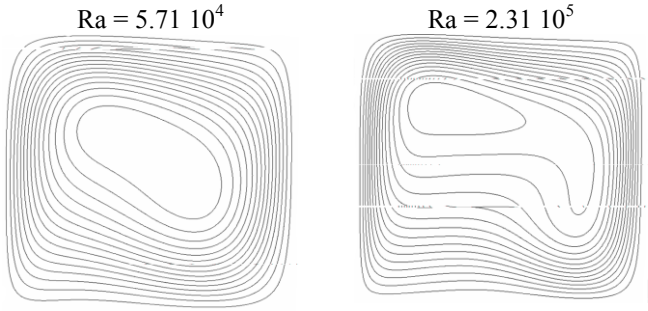

Fig.9 Numerical streamlines for l = H/4

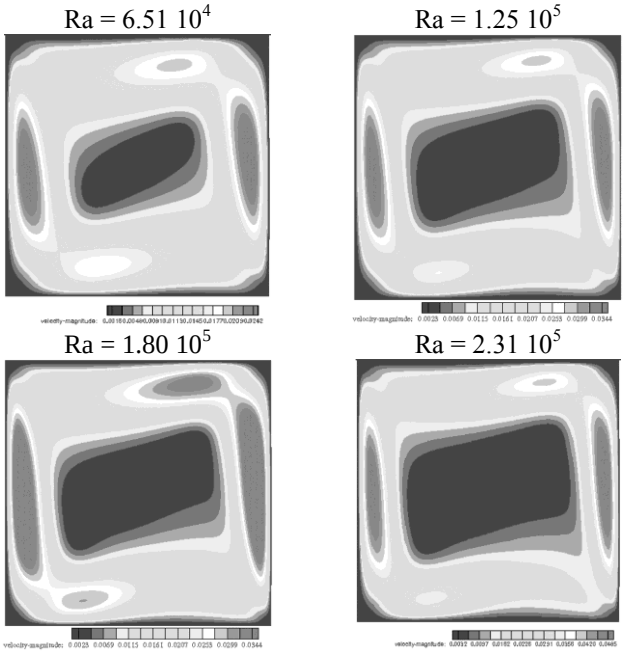

Fig.10 Numerical velocity maps for l = H

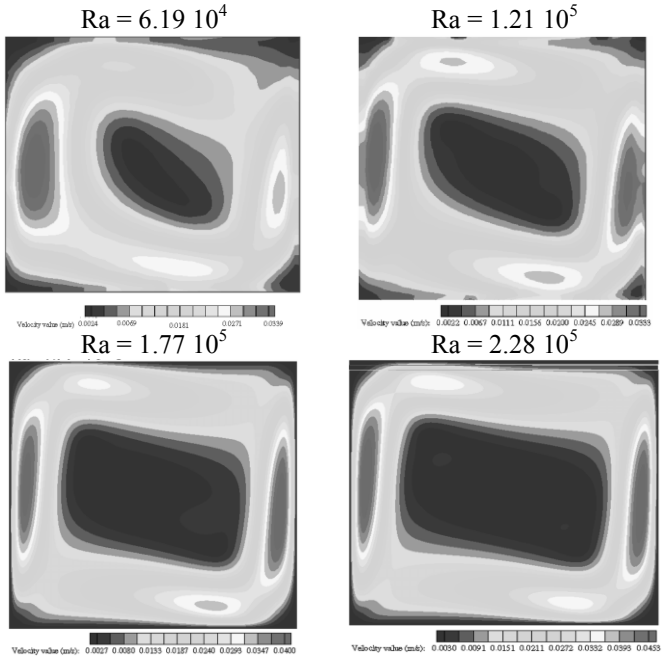

Fig.11 Numerical velocity maps for l H/2

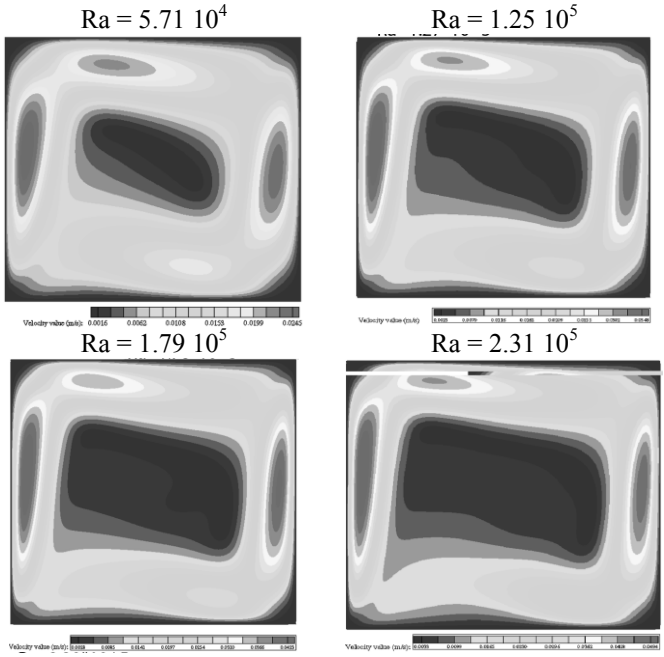

Fig.12 Numerical velocity maps for l H/4

A relationship between the average Nusselt number and the corresponding Rayleigh number is elaborated. The expression has the form:

$$Nu_{cal} = a \cdot Ra^b \qquad (7)$$

The correlation coefficients R^2 of each function are reported in Tables I and V. R^2 is an indicator that describes the fitting of the function to the experimental data, and is defined as follows:

$$R^2 = 1 - \frac{SSE}{SST} \qquad (8)$$

where

$$SST = (\sum_{j=1}^{n} k_j^2 + \frac{1}{n}(\sum_{j=1}^{n} k_j)^2 \qquad (9)$$

and

$$SSE = \sum_{j=1}^{n}(k_j - h_j) \qquad (10)$$

k_{js} are the n experimental values and hjs are the corresponding calculated value.

Experimental and calculated Nusselt numbers are shown in Tables II, III and IV for all configurations, while numerical and calculated Nusselt numbers are shown in Tables VI, VII and VIII.

Table I Experimental correlation parameters

	a	b	R^2
l = H	0.0292	0.4344	0.986
l = H/2	0.0073	0.5473	0.994
l = H/4 higher source	0.0432	0.3944	0.957
l = H/4 lower source	0.1088	0.3788	0.971

Table II Experimental and calculated Nusselt numbers for l = H

Ra	Nu_{exp}	Nu_{cal}	Δ(%)
4.020E+04	2.945	2.901	-1.51
6.490E+04	3.467	3.571	3.01
6.810E+04	3.610	3.647	1.02
1.020E+05	4.678	4.346	-7.09
1.261E+05	4.710	4.766	1.19
1.560E+05	5.025	5.227	4.03
1.770E+05	5.670	5.522	-2.61
1.790E+05	5.710	5.550	-2.81
1.980E+05	6.168	5.798	-6.00
2.302E+05	6.087	6.190	1.69
2.883E+05	6.710	6.826	1.73
3.206E+05	7.298	7.148	-2.05
3.896E+05	7.706	7.780	0.96

Table III Experimental and calculated Nusselt numbers for l = H/2

Ra	Nu_{exp}	Nu_{cal}	Δ(%)
6.19E+04	3.00	3.06	2.02
6.53E+04	3.16	3.15	-0.42
6.81E+04	3.23	3.22	-0.16
1.02E+05	4.05	4.02	-0.67
1.21E+05	4.61	4.42	-4.19
1.56E+05	4.99	5.08	1.56
1.77E+05	5.27	5.44	3.21
1.85E+05	5.57	5.57	0.04
1.98E+05	5.82	5.78	-0.63
2.28E+05	6.29	6.25	-0.67

Table IV Experimental and calculated Nusselt numbers for l = H/4

Ra	Nu_{exp} lower	Nu_{cal} lower	Δ(%)	Nu_{exp} higher	Nu_{cal} higher	Δ(%)
5.73E+04	6.71	6.90	2.87	3.07	3.25	5.92
7.81E+04	7.98	7.76	-2.73	4.01	3.67	-8.38
9.15E+04	8.52	8.24	-3.27	3.82	3.91	2.51
1.27E+05	9.43	9.33	-1.04	4.56	4.45	-2.40
1.40E+05	9.58	9.68	1.11	4.58	4.63	0.95
1.62E+05	10.15	10.23	0.82	4.88	4.90	0.42
1.78E+05	9.96	10.60	6.47	4.96	5.08	2.51
1.93E+05	10.88	10.93	0.47	5.33	5.25	-1.51
2.17E+05	11.64	11.43	-1.80	5.53	5.50	-0.64
2.30E+05	12.06	11.69	-3.10	5.52	5.63	1.91

Table V Numerical correlation parameters

	a	b	R2
l = H	0.0479	0.3986	0.978
l = H/2	0.0119	0.5068	0.997
l = H/4 higher source	0.1950	0.2661	0.961
l = H/4 lower source	0.4285	0.2533	0.969

Table VI Numerical and calculated Nusselt numbers for l = H

Ra	Nu_{exp}	Nu_{cal}	Δ(%)
4.014E+04	3.003	3.28	9.09
6.513E+04	4.187	3.97	-5.11
6.810E+04	4.080	4.04	-0.88
1.020E+05	4.690	4.75	1.30
1.251E+05	5.488	5.15	-6.10
1.560E+05	5.670	5.63	-0.75
1.770E+05	5.880	5.92	0.65
1.803E+05	6.221	5.96	-4.16
1.980E+05	6.176	6.19	0.20
2.312E+05	6.612	6.58	-0.44
2.783E+05	7.072	7.09	0.22
3.216E+05	7.365	7.51	1.95
3.984E+05	7.772	8.18	5.22

Table VII Numerical and calculated Nusselt numbers for l = H/2

Ra	Nu_{num}	Nu_{cal}	Δ(%)
6.19E+04	3.240	3.19	-1.50
6.53E+04	3.270	3.28	0.28
6.81E+04	3.340	3.35	0.29
1.02E+05	4.040	4.11	1.75
1.21E+05	4.520	4.48	-0.83
1.56E+05	4.994	5.10	2.09
1.77E+05	5.470	5.44	-0.64
1.85E+05	5.520	5.56	0.70
1.98E+05	5.840	5.75	-1.49
2.28E+05	6.200	6.18	-0.33

Table VIII Numerical and calculated Nusselt numbers for l = H/4

Ra	Nu_{exp} lower	Nu_{cal} lower	Δ(%)	Nu_{exp} higher	Nu_{cal} higher	Δ(%)
5.71E+04	6.96	6.87	-1.33	3.67	3.60	-2.03
7.79E+04	7.53	7.43	-1.33	3.78	3.91	3.32
9.13E+04	7.68	7.73	0.71	4.10	4.07	-0.64
1.25E+05	8.25	8.38	1.52	4.41	4.43	0.43
1.38E+05	8.45	8.59	1.63	4.67	4.55	-2.63
1.61E+05	8.98	8.93	-0.56	4.75	4.74	-0.29
1.79E+05	8.82	9.17	3.93	4.71	4.87	3.39
1.92E+05	9.31	9.34	0.25	4.82	4.97	3.01
2.19E+05	9.78	9.65	-1.29	5.15	5.14	-0.16
2.31E+05	10.15	9.78	-3.60	5.41	5.22	-3.60

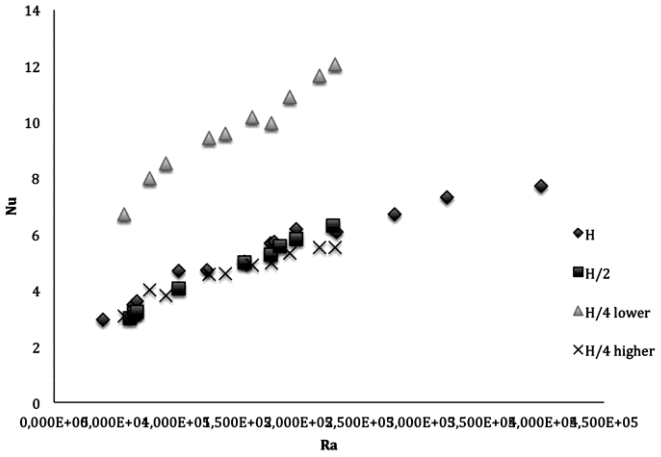

Fig.13 Experimental and Nu values for all configurations.

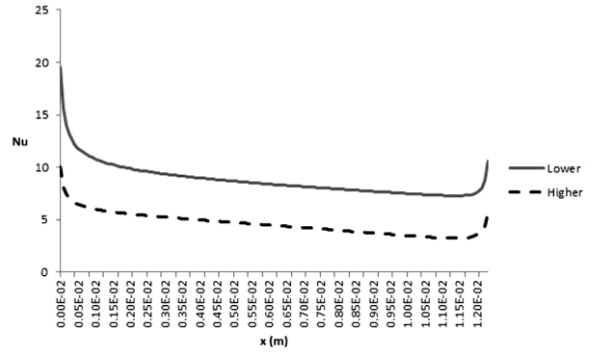

Fig.14 Numerical Nu values for the higher and lower strips for l = H/4.

For all configurations the differences between the numerical and calculated Nusselt numbers are less than 9.09%. In particular the worst numerical result (9.09%) is recorded for Ra = $4.014 \cdot 10^4$ (l = H). while the differences between the experimental and calculated Nusselt numbers are less than 8.38% for Ra = $7.81 \cdot 10^5$ (l = H).

In Fig. 13 it is possible to note that the dimension and number of the hot sources influence the thermal gradient and so the velocity field as indicated by the Nusselt numbers. In fact for l = H/4 the lower source has the higher heat transfer coefficient than the other two configurations. This fact is due to the upward moving plume from the lower source that impinges on the higher source and affects its heat transfer characteristics. The fact that the fluid arriving at the higher source is in motion means that the higher source is situated in what appears to be forced convection flow. On the other hand, the heat transfer at the lower source tends to increase the temperature of the fluid which reaches the higher source with a value that is higher than the one of the ambient fluid. Consequently, in this case, the buoyancy plume from the lower source decreases the heat flux of the higher source.

Fig. 14 shows the trend of the local Nusselt number along the higher and lower hot strip in the l=H/4 configuration.

V. Conclusions

The dimension and number of the sources influence the thermal gradient in the velocity field and so in this paper is carried out a study to evaluate the effect of the heat sources' dimension to have a better natural convective heat transfer in a square cavity and the results are presented.

This analysis is made up of two parts. The first step is characterized by an experimental study that is performed by a holographic interferometry and the second part is carried out with Fluent 12.1.4 software. A comparison between the experimental data and numerical ones presented good agreement for the Rayleigh number range from 10^4 to 10^6.

For all configurations, for Ra = $1 \cdot 10^5$ the heat transfer increases as the convection regime increases. For the l = H/2 at the highest Rayleigh numbers it is possible to see two vortexes but their size changes with the increase of the Rayleigh number, while for l = H and l = H/4 one vortex. The dimension and number of the sources influence the velocity field. In fact, analyzing the three different configurations it is possible to notice for each configuration an increase of Nusselt numbers and of the velocity values with the increase of the Rayleigh numbers. In particular, analyzing the velocity maps, it is possible to notice that the velocity fields of the l = H are faster than the l = H/2 ones, but the velocity fields of the l = H/4 concerning the lower source are faster than the all other ones. In fact for l = H/4 the lower source has the higher heat transfer coefficient than the other two configurations. This fact is due to the buoyancy plume from the lower source that decreases the heat flux of the higher source. The fact that is confirmed by the Nusselt numbers proves a better development of the natural convective heat transfer with the increase of the Rayleigh numbers in the l = H/4.

References

[1] P. Poulikakos. Natural convection in a confined fluid-filled space driven by a single vertical wall with warm and cold regions. ASME J. Heat Transfer 107. 1985. pp. 867–876

[2] Ishihara. R. Matsumoto. A. Senoo. Natural convection in a vertical rectangular enclosure with localizing heating and cooling zones. Heat Mass Transfer 36. 2000. pp. 467–472.

[3] O. Aydin and W.J. Yang. Natural convection in enclosures with localized heating from below and symmetrical cooling from sides. Int. J. Num. Methods Heat Fluid Flow. Vol. 10. No. 5. 2000. pp. 519-529.

[4] C.J.Ho and J.Y.Chang. A study of natural convection heat transfer in a vertical rectangular enclosure with two-dimensional discrete heating: effect of aspect ratio Int. J. Heat Mass Transfer 37 (6). 1994. pp. 917-925.
[5] M.M. Ganzorolli and L.F. Milanez. Natural convection in rectangular enclosures heated from below and symmetrically cooled from the sides. Int. J. Heat Mass Transfer. Vol. 38 No. 6. 1995. pp. 1063-73.
[6] E. Ntibarufata. M. Hasnaoui. E. Bilgen and P. Vasseur. Natural convection in partitione enclosures with localized heating. Int. J. Num. Meth. Heat Fluid. Vol. 3. 1993. pp. 133-143.
[7] M. Paroncini, F. Corvaro and M.M. De Padova, Study and analysis of the influence of a small heating source position on the natural convective heat transfer in a square cavity. Proceedings of the 4th WSEAS Int. Conf. on Heat Transfer, Thermal Engineering and Environment, Elounda, Greece, August 21-23, 2006. pp. 305 – 310.
[8] F. Corvaro and M. Paroncini, A 2D-PIV study and a numerical analysis of the natural convection in enclosures heated from below. Proceedings of the 2nd WSEAS Int. Conference on Applied and Theoretical Mechanics, Venice, Italy, November 20-22, 2006. pp. 136 – 141.
[9] C.S. Nor Azwadi and N.I. Nik Izual, Mesoscale Simulation of Natural Convection in an Inclined Square Cavity. Proceedings of the 9th WSEAS International Conference on Applications of computer Engineering, 2010. pp.164 – 169.
[10] C.S. Nor Azwadi and N.I. Nik Izual, Lattice Boltzmann Numerical Scheme for the Simulation of Natural Convection in an Inclined Square Cavity. WSEAS Transactions on Mathematics. Issue 6, Volume 9, June 2010. pp. 417 – 426.
[11] M. November and M.W. Nansteel. Natural convection in rectangular enclosures heated from below and cooled along one side. Int. J. Heat Mass Transfer. Vol.30. 1987. pp.2433-40.
[12] A. Raji. M. Hasnaoui and Z. Zrikem. Natural convection in interacting cavities heated from below. Int. J. Num. Meth. Heat Fluid. Vol.7. 1997. pp. 580-597.
[13] H. Tūrkoglu. N. Yūcel. Effects of heater and cooler location on natural convection in square cavities Numerical Heat Transfer. Part A 27. 1995. pp. 351-358.
[14] N. Nithyadevi. N. P. Kandaswamy. J. Lee. Natural convection in a rectangular cavity with partially active side walls. Int. J. Heat Mass Transfer 50. 2007. pp. 4688-4697.
[15] H. S. S. Chu. S. W. Churchill and S. V. Patterson. The effects of heater size. location. aspect ratio and boundary conditions on two-dimensional. laminar. natural convection in rectangular channels. ASME J. Heat Transfer 98. 1976. pp. 194-201.
[16] A. Valencia. R.L. Frederick. Heat transfer in square cavities with partially active vertical walls. Int. J. Heat Mass Transfer 32 (8). 1989. pp. 1567-1574.
[17] G. Nardini, M. Paroncini and R. Vitali. 4th International Conference on Fluid Mechanics and Heat & Mass Transfer (FLUIDSHEAT '13), Dubrovnik, Croatia, June 25-27, 2013. pp. 117 – 122.
[18] Zhao. Liu et al. Resonant response of fluid flow subjected to discrete heating elements. Energy conversion and management 48. 2007. pp. 2461-2472.
[19] Qi-Hong Deng. Fluid flow and heat transfer characteristics of natural convection in square cavities due to discrete source-sink pairs positions. Int. J. of Heat and Mass Transfer 51. 2008. pp. 5949-5957.
[20] "FLUENT User's Guide". Fluent Incorporated
[21] W. Hauf , U. Grigull. Optical methods in heat transfer, in: J.P.Harnett. T.F. Irvine Jr. (Eds). Advances in Heat transfer. Academic Press.